Surfaces and Interfaces xxx (xxxx) 101888

Contents lists available at ScienceDirect

Surfaces and Interfaces

journal homepage: www.elsevier.com/locate/surfin

# Investigation of hydroxyapatite (HAP) containing coating on grade 2 titanium alloy prepared by plasma electrolytic oxidation (PEO) at low voltage

Lorena Kostelac [a], Luca Pezzato [a,*], Alessio Giorgio Settimi [a], Mattia Franceschi [a], Claudio Gennari [a], Katya Brunelli [a], Chiara Rampazzo [b], Manuele Dabalà [a]

[a] Department of Industrial Engineering, University of Padova, Via Marzolo 9, 35131 Padova, Italy
[b] Department of Biology, University of Padova, Via Ugo Bassi 58/B, 35131 Padova, Italy

ARTICLE INFO

*Keywords:*
Plasma electrolytic oxidation (PEO)
Titanium
Hydroxyapatite
Biocompatibility

ABSTRACT

In this work, plasma electrolytic oxidation (PEO) process was used to produce bioactive coatings, mainly composed by hydroxyapatite (Hap) and titanium oxide, on grade 2 titanium alloy. All PEO treatments were carried out using a maximum voltage of 315 V, a lower value in comparison with the works present in literature, thus resulting a more environmentally friendly process. The effects on the PEO coatings of KOH addition to electrolyte and of working in direct or pulsed current mode, were also investigated. The morphology and elemental composition of the coatings were characterised by scanning electron microscopy (SEM), whereas the phase analysis was carried out with X-ray diffraction (XRD). The corrosion resistance properties were investigated by open circuit potential measurements, potentiodynamic polarization (PDP), and electrochemical impedance spectroscopy (EIS) tests. Moreover, cell-adhesion biological tests were performed. SEM analysis evidenced the presence of needle-shape crystals of hydroxyapatite, as confirmed by XRD, that totally or partially filled the pores of PEO layer. The corrosion test showed an improvement in the corrosion behaviour of the PEO coated samples in comparison with the untreated sample. Cell-Adhesion biological tests evidenced excellent cytocompatibility of the coatings with human cells and an improvement in the cell adhesion in comparison with the untreated sample.

## 1. Introduction

The most promising implantable metallic biomaterials are titanium and its alloys [1, 2] due to its good properties such as high biocompatibility with bone cells and muscle, good corrosion resistance in human body fluid, good mechanical properties, low density, chemical inertness, and no-toxicity [3–5]. Titanium and its alloys are often used as materials in the biomedical field [5–8], especially as orthopaedic and dental implant materials [3,4,16–18,5,9–15]. Many investigations have been performed to improve mechanical properties, osseointegration and fixation between bone structures and the implant. Particular attention has been paid in combining surface modification, such as porosity [19] and roughness [7], and bioactive coatings on titanium-based alloy surfaces [14]. The most commonly used bioactive coating is composed of Hap [20]. Hap ($Ca_{10}(PO_4)_6(OH)_2$) is a naturally occurring mineral form of calcium apatite and a major mineral component of bones and teeth [10,16,21]. When it is synthetically produced on the surface of titanium, it can promote bioactivity and improve the connection with bone tissue [4,18]. $TiO_2$ coatings on Ti have also been produced in recent years to improve the corrosion resistance of Ti [18]. There are several ways to form Hap and $TiO_2$ on the surface of titanium and its alloy. These methods include techniques such as ion beam-assisted deposition, plasma spray deposition, electrophoretic deposition, pulsed laser physical vapour deposition, plasma electrolytic oxidation, and magnetron sputtering deposition, etc. Each of these methods has its own advantages and disadvantages, but amongst them, plasma electrolytic oxidation (PEO) stand out [11,22]. PEO is an electrochemical surface treatment technique, that is considered as one of the most useful methods for surface modification of titanium alloy, because it can produce porous microstructure at the implant surface, which not only improves corrosion behaviour [23], but also enhances implant fixation to the bone [16]. Coating formation by PEO is based on polarizing the metal over the dielectric breakdown voltage in a suitable electrolyte. A wide range of process conditions are available for formation of the coatings,

* Corresponding author.
*E-mail address:* luca.pezzato@unipd.it (L. Pezzato).

https://doi.org/10.1016/j.surfin.2022.101888
Received 22 December 2021; Received in revised form 28 February 2022; Accepted 15 March 2022
2468-0230/

including DC and AC current modes [24]. Main characteristics of PEO process is the possibility to proper functionalize the coatings thank to the addition of particles into the electrolyte [25] or thank to interactions between the electrolyte and the substrate [26]. In this way the coating resulted composed not only by the oxide of the substrate but also by other compounds, that can confer to the coating proper characteristics, for example cytocompatibility [27] or bactericidal effect [28,29]. The electrolyte employed in the formation of PEO coatings on Ti alloys are usually basic aqueous electrolytes but also other innovative solutions, such as molten salts electrolytes [30,31], have been recently studied in order to further functionalize the obtained coatings.

Biocompatible Hap-containing coatings were already produced on titanium alloys by PEO in the literature [14,32,33]. In particular, the biocompatibility was obtained either by addition of proper particles into the electrolyte [34,35] or by proper formulation of the electrolyte in order to directly form Hap during the treatment. In this second case, specific compounds should be added into the electrolyte, in particular Ca and P compounds as deeply studied by Molaei et al [36]. However, in literature, as reported for example in the comprehensive review work of Pesode et al. [37] or in the book [38], PEO coatings on Ti alloys are produced at high voltages, between 500 and 800 V, with very high energy consumption. Studies about the use of lower voltages during PEO process were already performed on Al alloys [39,40], whereas the production of energy efficient PEO coatings on Ti alloys is not yet reported in literature.

The aim of this study was to produce Hap and $TiO_2$ coatings on Ti grade 2 alloy using a PEO process working at low voltage, to reduce energy consumption. Moreover, the influence of different process parameters (addition of KOH to electrolyte, use of direct current mode or pulsed current mode) on the PEO coatings was studied.

## 2. Materials and methods

### 2.1. Titanium alloy and PEO conditions

In this study, cylindrical samples (10 × 10 mm) of titanium alloy (Grade 2) were used as a substrate for PEO process. Before the PEO treatment the samples (which were marked as A, B, C, D) were polished according to the standard metallographic techniques (grinding with abrasive papers 320, 500, 800, 1200 and 4000 grit and polished with clothes with 0.2 μm of colloidal silica) and after cleaned with distilled water and degreased with ethanol by ultrasound for 5 min. The electrolyte consisted of an aqueous solution of calcium acetate hydrate ($Ca(CH_3COO)_2$ x $H_2O$), sodium phosphate monobasic ($NaH_2PO_4$ x $H_2O$), potassium hydroxide (KOH) in various concentrations depending on the sample (reported in Table 1) and was maintained at room temperature with a thermostatic bath. The PEO equipment was composed of a Direct Current (DC) power supply (TDK-Lambda 400 V/8A), a stainless-steel container as well as cooling and stirring systems. The titanium substrate was used as anode, while the stainless-steel container was used as cathode. The treatments were all performed in galvanostatic mode at the current densities reported in **Table 1**; in the case of the pulsed mode (sample D) the treatment was performed with pulsed unipolar current with a frequency of 20 Hz and a duty cycle of 50% (for generating a pulsed PWM (Pulse Width Modulation) signal, it was used a supply, based on a relay technology, that opens and closes an electric contactor). The maximum voltage, for all the samples, was 315 V, in order to reduce energy consumption of PEO process. The other parameters of synthesis are given in **Table 1.** After the PEO treatment the samples were washed with distilled water and dried. From Table 1 can be noted that samples A and B were produced with similar parameters in terms of electrolyte composition, current density and treatment time. In detail, sample B was obtained with a slightly lower current density, to decrease the intensity of the sparks, compensated by a slightly higher treatment time to obtain a comparable coating thickness. In samples C and D, with the aim of energy saving, KOH was added to electrolyte to reduce the resistance of the solution, stabilize the discharges and reduce the breakdown potential [41]. The addition of KOH, in fact, thanks to the reduction of the solution resistance, reduced the treatment time in sample C and sample D, in comparison with sample A and B. The difference between samples C and D was the current mode, with sample D produced in pulsed current mode, with increased treatment time in comparison with sample C, due to compensation of the off-time present in pulsed mode.

**Table 1**
PEO parameters of synthesis of various bioactive coatings on titanium substrate.

| Sample | Electrolyte | Time (min) | Pulsed mode | pH | Current density (A/cm$^2$) |
|---|---|---|---|---|---|
| A | 0.120 M $NaH_2PO_4$ x $H_2O$<br>0.260 M $Ca(CH_3COO)_2$ x $H_2O$ | 9 | - | ~7 | 1.273 |
| B | 0.120 M $NaH_2PO_4$ x $H_2O$<br>0.200 M $Ca(CH_3COO)_2$ x $H_2O$ | 11 | – | ~7 | 1.061 |
| C | 0.120 M $NaH_2PO_4$ x $H_2O$<br>0.200 M $Ca(CH_3COO)_2$ x $H_2O$<br>0.143 M KOH | 2 | – | ~10 | 1.273 |
| D | 0.120 M $NaH_2PO_4$ x $H_2O$<br>0.200 M $Ca(CH_3COO)_2$ x $H_2O$<br>0.143 M KOH | 5 | + | ~10 | 1.273 |

### 2.2. Characterization of bioactive coatings on titanium substrate

A Cambridge Stereoscan 440 scanning electron microscope (SEM) (Leica Cambridge Ltd, Cambridge, England) equipped with a Philips PV9800 EDS was used to analyse the surface and the cross section of the bioactive coatings. SEM analysis were performed on the surfaces to see the morphology and distribution of both oxides and Hap coatings and on the cross sections to analyse thickness and uniformity of the protective layer. Additionally, both SEM cross-sectional and surface micrographs were linked to EDS elemental maps, to see the elemental distribution in both PEO and Hap layers. The samples for cross sectional analysis were previously mounted in epoxy resin and polished with standard metallographic technique (previously described) before observation.

X-ray diffraction (XRD) measurements were performed on the surface of the samples, in order to characterize the phases, present in the coating, with a Siemens D500 X-ray diffractometer (Munich, Germany) using Cu Kα radiation with 2θ ranging from 20° to 60° (0.05° step size and 5 s counting time per step) working at 40 kV and 30 mA with Bragg-Brentano geometry.

### 2.3. Electrochemical measurements

In order to detect the differences in corrosion resistance amongst coated samples, electrochemical measurements were performed. The corrosion behaviour was evaluated with OCP measurements, potentiodynamic polarization test (PDP) and electrochemical impedance spectroscopy tests (EIS). OCP measurements, PDP and EIS tests were performed using as electrolyte simulated body fluid (SBF) solution at 37 °C (SBF, composition: 1,5881 g/L NaCl, 0,0709 g/L $NaHCO_3$, 0,0746 g/L KCl, 0,0492 g/L $Na_2HPO_4$, 0,0617 g/L $MgCl_2$, 0,0403 g/L $CaCl_2$, 0,0171 g/L $CaSO_4$). In the literature [7,11,42] it can be found that SBF was often used as electrolyte for electrochemical measurements to simulate biomedical applications. In particular SBF was used due to the

proximity of its ionic composition to the ionic composition of human blood plasma [11]. For the OCP measurements and the PDP tests an AMEL 2549 potentiostat (Amel S.r. l., Milano, Italy) was employed. A saturated calomel electrode (SCE) was used as a reference electrode and platinum one as a counter electrode. OCP test consisted in monitoring the value of the open circuit potential for 3 h. The PDP test was performed with a scan rate of 0.5 mV/s and at least three measures for each sample were recorded to assure reproducibility. The EIS measurements were performed with a Materials Instrument Spectrometer connected with the AMEL 2549 potentiostat working at the open circuit voltage (OCV) after 1 h of OCV stabilization, using a range of frequencies between $10^{-2}$ Hz and $10^{5}$ Hz and a perturbation amplitude of 10 mV. Also, in this case the measures were repeated at least three times and the experimental data were fitted with the software Z-View using proper equivalent circuit.

### 2.4. Cell adhesion test

To evaluate cell adhesion, immortalized skin fibroblasts were seeded on titanium alloy discs of 10 mm in diameter and 1 mm in thickness. Prior cell seeding, each titanium disc was sterilized for 15 min by ultraviolet irradiation, placed in a well of a cell culture plate (24 flat bottom well, Corning Life Sciences), washed twice with Phosphate Buffered Solution pH7.4 (PBS) and let equilibrate 3 h in 1 ml DMEM supplemented with 10% fetal Bovine Serum (FBS). Next, $5.0 \times 10^{4}$ skin fibroblasts were seeded in each disc and incubated for 2 days at 37 °C, 5% $CO_2$ atmosphere in presence of DMEM with 10% FBS. After the culturing, the cells on substrate were washed twice with Balanced Salt Solution (HBSS, Invitrogen) and stained with 2 μM calcein acetoxymethylester (Calcein-AM, Biotium Inc., Fremont, CA, USA) in HBSS, in the dark at 37 °C and 5% CO2. After 30 min, staining solution was removed and the cells were washed three times with PBS and preserved in PBS solution until observation with Leica DM4000B fluorescent microscope using a GFP filter.

## 3. Results and discussion

### 3.1. SEM characterization of the bioactive coatings

SEM analysis were first performed in order to characterize the morphology of the bioactive coatings. **Fig. 1.** shows SEM micrographs at low magnification of the surfaces of the PEO treated specimens where highly porous layers can be observed. The pore structure is characteristic for the oxide layer formed by PEO treatment on titanium alloys [10]. This can be in particular recognized in sample C and D (**Fig 1.C and 1.D**), while needle shape crystals above the pores, that are the characteristic microstructure for the hexagonal Hap [21], can be observed in sample A and B (**Fig 1.A and 1.B).** The Hap crystals partially or totally filled the pores that characterize the PEO layer. In particular, in all the samples were present pores with dimensions range up to a size of about 1 μm. The surface pores are caused by the plasma discharge, the intensity of which depends by the PEO treatment parameters. The diameter of the pores and the coating roughness increase with greater current densities, applied potential and electrolyte concentration [16]. The resulting microstructure was very rough for all four samples and it can be benefit, since it can promote the intergrowth of natural bones and accelerate interfacial bonding between the implants and the natural bones [43].

In **Fig. 2,** where SEM images taken at higher magnification are shown, Hap needle shape crystals be observed above and around the pores. In particular, it can be clearly noted that Hap are present in all four samples. The concentration of Hap crystals was higher in sample A where it covered the entire surface of the porous structure, whereas resulted lower in sample C and D. Also, SEM-EDS elemental mapping was performed on the surfaces of the samples with images at higher magnification and the results are reported in **Fig. 3.** EDS elemental mapping confirmed that the crystals were mainly composed by Ca, P and O, indicating that their composition is compatible with the one of Hap.

From the observation of Fig. 3 it can be clearly noted also a remarkable difference amongst sample A and the other samples. In fact, in sample A, Ca and P resulted uniformly distributed on the surface, confirming the fact that in this sample the Hap crystals completely covered the surface. In the other samples can be observed the presence of zones where Ti and O are more visible, thus indicating the partial absence of

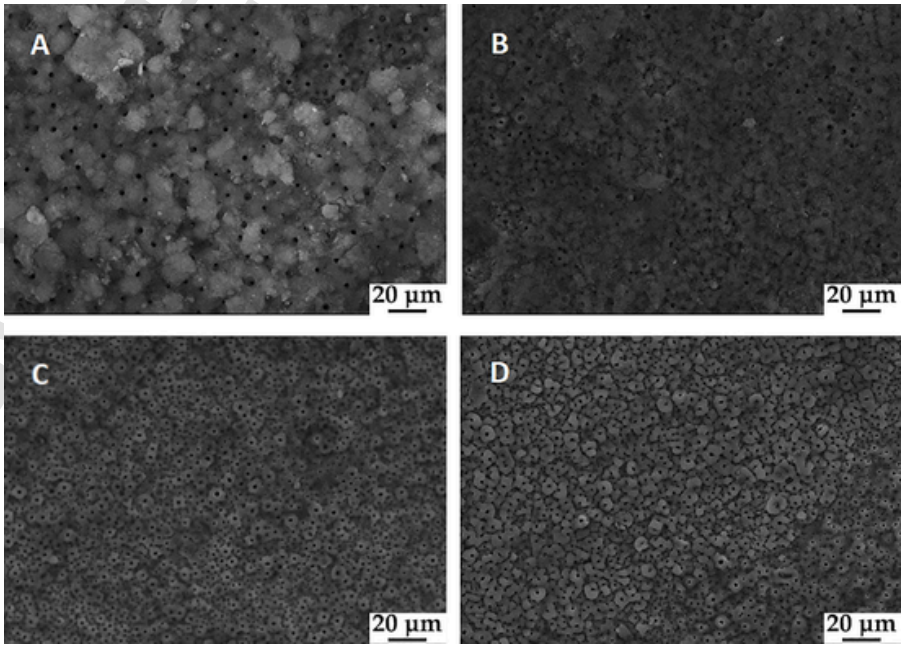


**Fig. 1.** SEM plan-view images at low magnification for sample A and sample B, where Hap crystals can be foreseen and for sample C and sample D, where a porous structure, characteristic of the oxide, can be seen. The letters in the upper left corner indicate the corresponding samples.

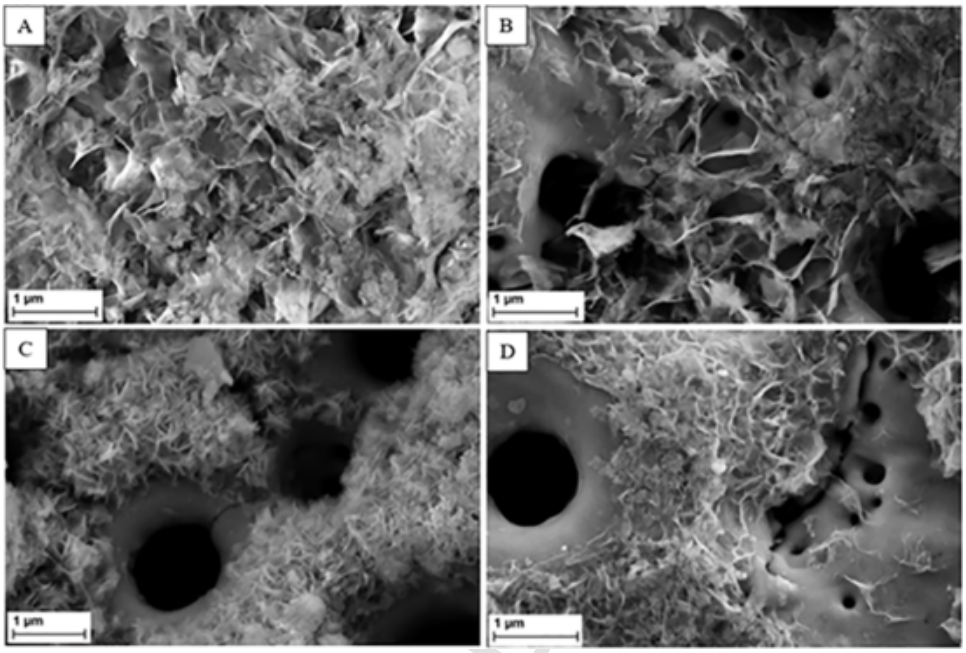


**Fig. 2.** SEM micrographs of samples A, B, C and D, where pores and Hap needle shape crystals around them can be observed at higher magnifications. The letters in the upper left corner indicate the corresponding samples.

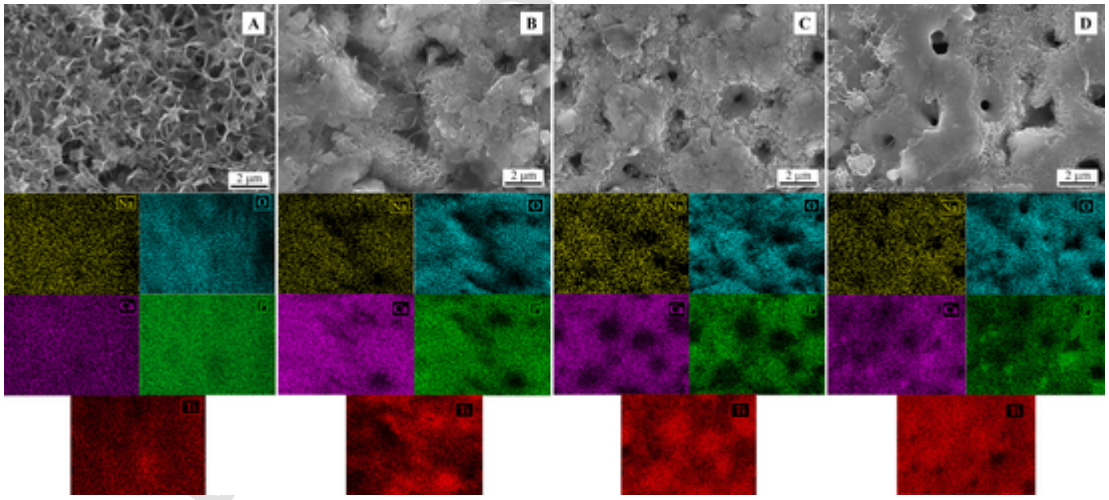


**Fig. 3.** SEM-EDS elemental mapping performed on the high magnification images of the surfaces of the coated samples. Red colour corresponds to Ti, green to P, purple to Ca, light blue to O and yellow to Na. The letters in the upper right corner indicate the corresponding samples.

Hap crystals and the presence of the titanium dioxide, characteristic of PEO coating.

Coatings of all four samples consist generally of two or three layers, which can be seen summarized in the SEM cross-sectional micrograph of sample A (**Fig 4**). It can be noted the presence of an inner compact layer, very thin and characteristic of PEO coatings [44], another layer, which is the oxide layer, full of pores (the so called technological layer) and finally Hap layer in the form of needle shape crystals (present only in the samples A and B).

Cross sectional micrographs of all the samples are reported in Fig. 5. The three-layered structure previously described can be clearly observed in sample A and sample B with a PEO layer about 8 μm thick and a Hap layer about 3 μm thick. In sample C and D, characterised by a PEO layer of about 8 μm thick, Hap layer was not present, in agreement with the observation carried out on the surface. It can be noted in all the treated samples a similar thickness of the PEO layer, as expected from the selection of the experimental conditions. In fact, the decrease in the treatment time in sample C and D was compensated by the addition of KOH that reduced the resistance of the solution. This fact, together with the maximum operating voltage that remained at 315 V, allowed to obtain coatings with the same thickness reducing the treatment time.

To further clarify the elemental distribution in the bioactive coating, SEM-EDS mapping was performed also along the cross section, and the results are reported in **Fig 5**. It can be observed that calcium and phosphorus were present in all four samples confirming the presence of Hap in all the produced samples. In particular, in all the samples Ca and P were present in the whole coating due to the previously reported sealing effect of the pores. In samples A and B, it was also confirmed the presence of an external layer rich in Ca (and partially P), whereas this was not present in sample C and D, where Ca and P only filled the pores of the PEO coating. However, in this last two samples P and Ca were clearly more concentrated in the external part of the PEO layer confirming the sealing of the pores with Hap-based compounds.

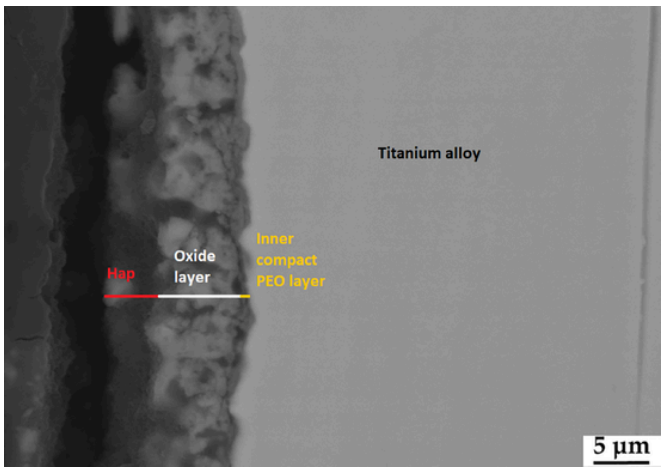


**Fig. 4.** SEM cross-sectional micrograph of sample A that shows the presence of three layers in the prepared bioactive coatings (inner, compact layer, oxide layer and Hap layer).

### 3.2. XRD characterization of the bioactive coatings

Fig. 6. presents the results of XRD phase composition analysis for the coated samples. The coatings resulted in all the cases composed by a mixture of Hap (Hap), anatase and rutile whereas titanium peaks comes from the reflection of the substrate. Table 2. shows the proportion of each crystalline phase in the coating for all the samples, obtained with the Rietveld method. It can be observed that the highest percentage of Hap was present in sample A and decreased in sample B, C and D. This agreed with SEM results, that evidenced in sample A an almost total surface coverage of Hap above and around the pores. In sample B instead the PEO layer was already visible and in sample C and D a relevant part of the surface was not covered by Hap. The amount of Rutile changed remarkably between the couple of sample A-B, where it is very low (3.9 and 0.9%), and the one C-D, where was about 20%. This can be probably related to the presence of KOH in the electrolyte for samples C-D that increased the conductivity of the solution, producing an increase in the intensity of sparks and a consequent higher formation of Rutile due to higher local temperatures [45].

### 3.3. Electrochemical characterization of the bioactive coatings

The corrosion resistance of the four coated samples and of uncoated titanium (used as reference) was evaluated with OCP measurements, PDP and EIS tests. The trend of the OCP during 3 h of monitoring can be found in Fig. 7 and the values at which the OCP stabilized are reported for the different samples in Table 3.

From OCP measurements can be observed that sample C was characterized by a stabilization of the OCP at nobler values, and therefore it is the more promising in terms of corrosion performances. In fact, for this sample can be observed and increase in the value of the OCP with the time and a stabilization at a value of −0.182 V, thus indicating that the barrier effect of the coating was not reduced during the 3 h of immersion. Sample D was instead the sample characterized by the lower corrosion resistance, in fact the OCP decreased and at the end stabilized at the value of −0.379 V, the same of the untreated Ti, thus suggesting that after 3 h of immersion in SBF the protective layer was less effective against corrosion. Sample A and sample B showed and intermediate behaviour with the OCP value that stabilized respectively at −0.331 V and −0.347 V, higher than the untreated Ti but lower than sample C.

The PDP curves of pure titanium and of coated samples, obtained in SBF solution at 37 °C, are plotted in **Fig 8** whereas $E_{corr}$ and $i_{corr}$ values, graphically extrapolated from the curves, are reported in **Table 3.** Both, coated samples and pure titanium showed an active to passive transition behaviour. It can be clearly observed that all the coated samples exhibited improved corrosion performances (both in term of corrosion currents and potentials) in comparison with the uncoated titanium sample. In fact, as can be observed in Table 3, the corrosion potential increase of about 0.4 V and the corrosion current density decrease up to two order of magnitude in the coated samples (in the order of $10^{-8}$ A/cm$^2$) in comparison with the uncoated one (in the order of $10^{-6}$ A/cm$^2$). Considering that PEO coatings are thick ceramic insulant coatings, [33], PDP were employed only for qualitative observation amongst coatings and pure titanium and cannot be employed to perform quantitative analysis amongst the different coated samples. However, from a first semi quantitative observation of the data it seems that the more promising samples in terms of corrosion performances are sample B, C and D due to the lower values of corrosion current densities.

In order to deeply investigate the corrosion properties of the obtained samples, EIS tests were also performed in SBF solution at 37 °C. Results from the EIS test are presented in form of Nyquist plot (**Fig. 9a**),

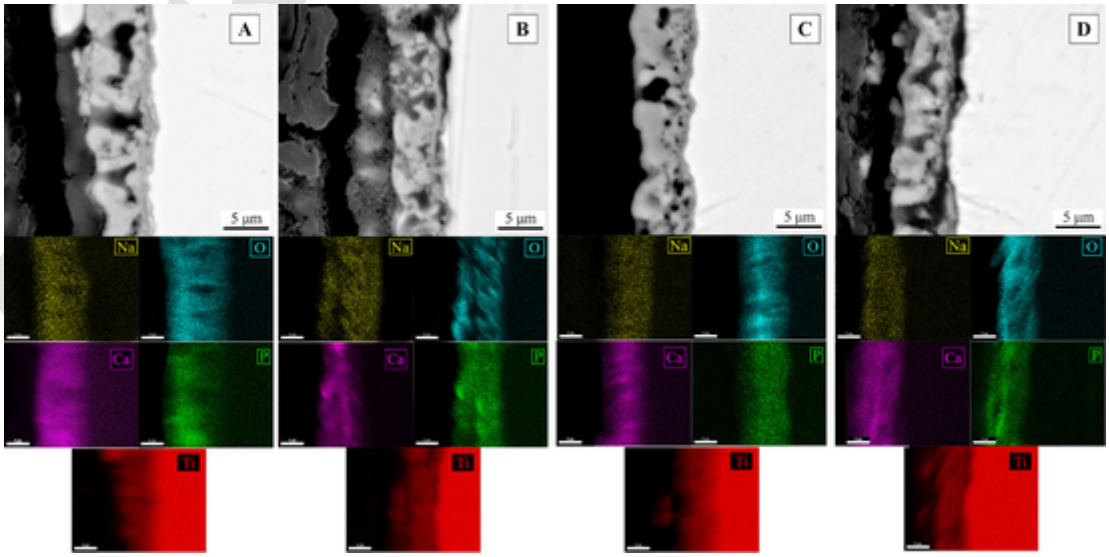


**Fig. 5.** SEM cross-sectional micrographs and EDS elemental mapping of the samples A, B, C and D. Red colour correspond to Ti, green to P, purple to Ca, light blue to O and yellow to Na. The letters in the upper right corner indicate the corresponding samples.

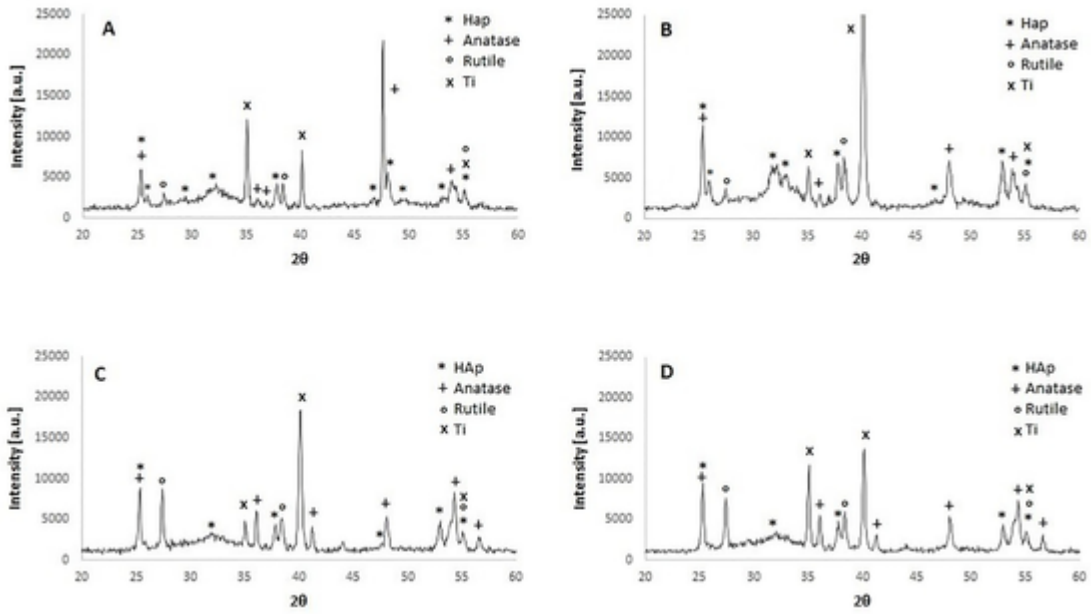


**Fig. 6.** Results of XRD analysis for samples A, B, C and D. The letters in the upper left corner indicate the corresponding samples.

**Table 2**
Quantitative evaluation of the phases in sample A, B, C and D, performed with the Rietveld method.

| Sample | HAp(%) | Anatase(%) | Rutile(%) | Ti(%) |
|---|---|---|---|---|
| A | 72.3 | 14.6 | 3.9 | 18.5 |
| B | 58.1 | 14.1 | 0.9 | 26.8 |
| C | 40.4 | 16.2 | 20.2 | 23.1 |
| D | 36.1 | 18.6 | 20.0 | 25.4 |

Bode modulus plots (Fig 9**b)** and Bode phase plot (Fig 9**c).** From the Nyquist and Bode modulus plots, the samples A and C had the highest impedance value at low frequency ($10^{-2}$ Hz), one order of magnitude higher than sample D. This indicates better corrosion resistance of samples A and C compared to samples B and D. From the Bode-phase plot, two-time constants can be observed in all four samples, the first in the high-frequency region with minimum at about $10^{3}$ Hz and the second one in the low-frequency region with minimum at about $10^{-1}$ Hz. The presence of these time constants indicates the presence of two layers, an outer porous one (bend in the high frequency region) and an inner compact layer (bend in the low frequency region). These results are in accordance with the ones in the literature [11] and with the previously reported SEM observations. The Hap layer and the oxide layer can be considered in fact as one unique porous layer from the electrochemical point of view, due to the fact that the Hap layer was not compact and filled the pores that characterize the PEO coating.

Differences in the phase angle of sample D, at low frequencies, can be attributed to different process parameters of PEO process because only sample D was prepared in pulsed current mode. The time constant at low frequency is associated with the inner PEO layer and so it possible to conclude that with the pulsed mode a more porous inner layer

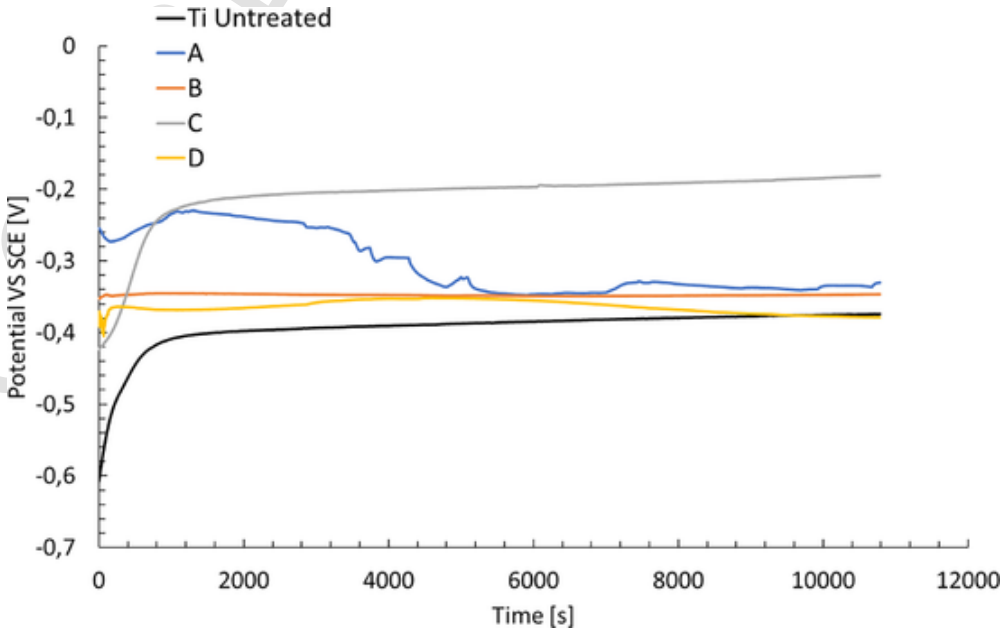


**Fig. 7.** OCP curves of the coated samples A, B, C, D and of pure Ti. Test Electrolyte: SBF at 37 °C.

**Table 3**
Electrochemical data graphically extrapolated from OCP measurements and PDP tests performed in SBF solution at 37 °C.

| | A | B | C | D | Ti Untreated |
|---|---|---|---|---|---|
| $E_{corr}$ [V vs SCE] | −0.292 | −0.372 | −0.401 | −0.238 | −0.770 |
| $i_{corr}$ [A/cm$^2$] | $1.5 \times 10^{-7}$ | $4.4 \times 10^{-8}$ | $6.5 \times 10^{-8}$ | $5.0 \times 10^{-8}$ | $1.45 \times 10^{-6}$ |
| OCP [V vs SCE] | −0.331 | −0.347 | −0.182 | −0.374 | −0.379 |

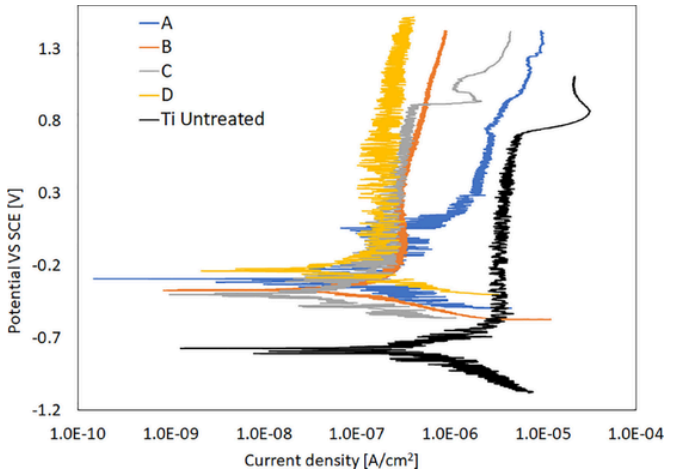


**Fig. 8.** Potentiodynamic polarization curves of the coated samples A, B, C, D and of pure Ti. Test Electrolyte: SBF at 37 °C.

can be obtained which contributes to poorer corrosion properties of the coatings, as evidenced by EIS tests.

EIS results were also fitted with the equivalent circuit shown in Fig. 10 with Z-view software. The choice of the circuit was performed accordingly to the literature, and in particular with circuits employed for PEO coatings [11,44]..

The electrical circuit consists of two parallel R-CPE where each of them represents one layer of the PEO coating (inner compact layer and oxide layer). In fact, the Hap layer should not be considered separately from the PEO layer from the electrochemical point of view due to the fact that, as evidenced in Fig. 2, it was not a compact layer but was composed by needle shape crystals, which do not act as separate barrier against corrosion but fill the pores of the oxide layer. Considering this, the contribution of the Hap layer was inside the one of the porous oxide layer that resulted, depending on the sample, partially or totally filled by Hap.

Since the capacitance measurement often is not ideal, CPE (constant phase element) was used. Considering in detail the physical meaning of each element, $R_3$—$CPE_2$-chain represents the porous part of the coating, $R_2$ is the resistance of the dense barrier layer, and $CPE_1$ is the element, responsible for the whole coating thickness

The calculated parameters of the circuit elements for the samples A, B, C and D with the corresponding electrical circuit can be found in the Table 4. Low values of chi-squared ($\chi^2$) indicates a good fitting quality as well as the good correspondence between dots and lines in Nyquist and Bode plots.

From the calculated data it can be seen that the value of $R_3$ is several magnitudes higher than the value of $R_2$. This is clearly linked with the previously reported SEM observation where the pores of PEO layer were filled and sealed by Hap crystals. This produced a remarkable increase in the barrier effect of the porous layer because the electrolyte cannot penetrate easily into the pores, consequently increasing the corresponding value of $R_3$.

The $R_3$ values of samples A and C are similar and were the ones characterized by the higher resistance. The $R_3$ value of sample D was much lower than all other samples and this agrees with the SEM and XRD observation that evidenced the presence of less Hap and so less sealing of

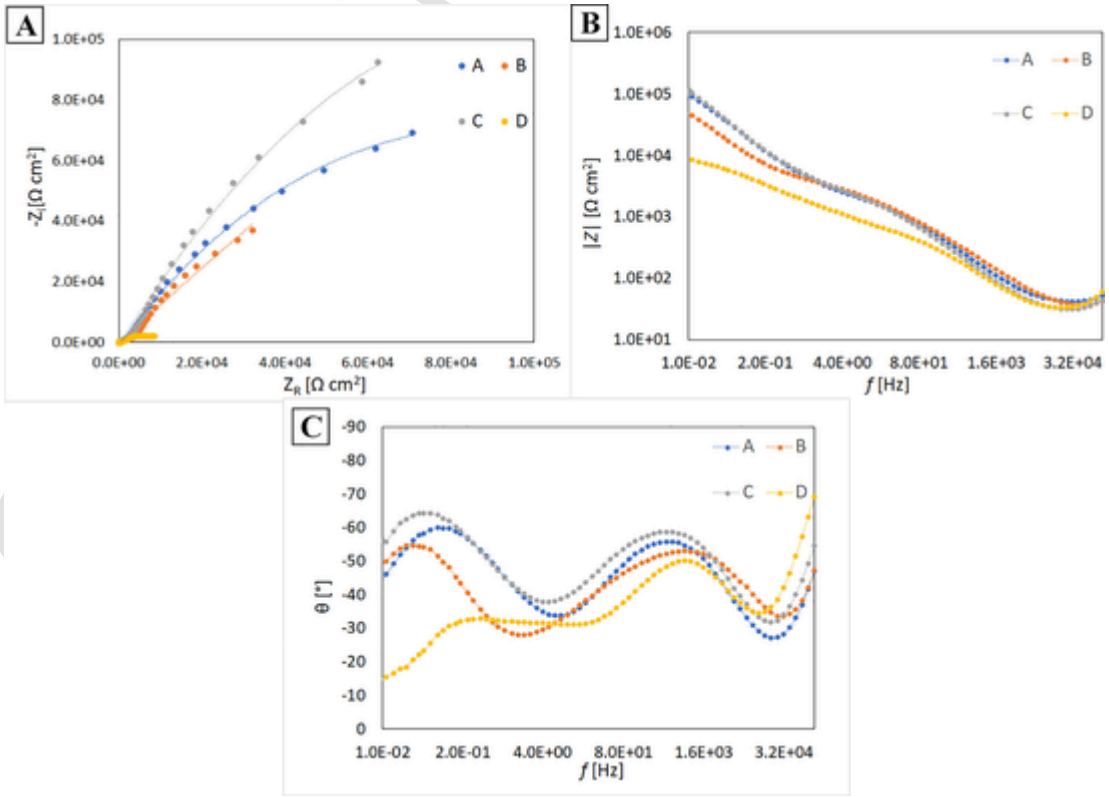


**Fig. 9.** Results of EIS tests in form of **a)** Nyquist Plot (ImZ vs ReZ) **b)** Bode Modulus plot (impedance vs frequency ($|Z|$ vs $f$)) and **c)** Bode phase plot (phase angle vs frequency ($\theta$ vs $f$)) for all coated samples in SBF solution at 37 °C. Dots represent experimental data whereas lines the result of the fitting.

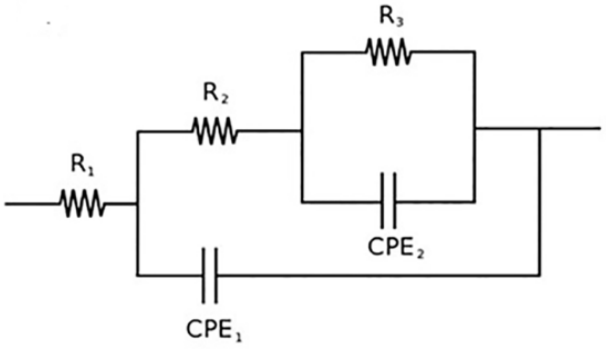


**Fig. 10.** Equivalent electrical circuits employed to fit the EIS data.

**Table 4**
Fitted results of the experimental EIS data of the coated samples A, B, C, D in SBF solution at 37 °C.

| | A | B | C | D |
|---|---|---|---|---|
| $R_1$ [Ω cm$^2$] | 50 | 48 | 40 | 42 |
| $R_2$ [Ω cm$^2$] | 1800 | 4302 | 1750 | 490 |
| $R_3$ [Ω cm$^2$] | $1 \times 10^5$ | $3.5 \times 10^4$ | $9.8 \times 10^4$ | 3474 |
| $Q_1$ [F Hz$^{1-n}$] | $5.74 \times 10^{-6}$ | $2.12 \times 10^{-5}$ | $3.1 \times 10^{-5}$ | $7.63 \times 10^{-6}$ |
| $n_1$ | 0.83 | 0.66 | 0.77 | 0.83 |
| $Q_2$ [F Hz$^{1-n}$] | $7.81 \times 10^{-5}$ | $1.31 \times 10^{-4}$ | $9.36 \times 10^{-5}$ | $1.45 \times 10^{-5}$ |
| $n_2$ | 0.61 | 0.80 | 0.65 | 0.66 |
| $\chi^2$ | 0.00035 | 0.00083 | 0.00085 | 0.00089 |

the pores; in particular, probably in sample D some pores remained unsealed and this caused a penetration of the electrolyte into the pores.

Considering the values of $R_2$, that represents the barrier layer, also in this case the sample D was the one characterized by the lower values. This fact was correlated with the results shown in the Bode plot and was related to a different microstructure of the inner layer, due to the pulsed current mode employed. The results of the EIS tests resulted also in accordance with the ones of the OCP measurements where was evidenced that sample C was the one characterized by the higher corrosion properties.

### 3.4. Cytocompatibility tests

Cell migration and adhesion on an implant are required to form tissue. The proliferation and differentiation of mammalian cells depend not only on the chemical composition of the phase or oxide layer formed on a surface but also on the pore size and surface roughness [23]. To confirm the cytocompatibility of the obtained Hap coatings on the surface of the titanium alloy obtained by PEO, a cell adhesion-test was performed. Human skin fibroblasts were incubated with titanium alloy discs of 10 mm in diameter and 2 mm in thickness for 48 h after which they were stained with Calcein-AM to visualize live cells onto the titanium substrates. Indeed, Calcein-AM is a non-fluorescent cell permeable compound that when hydrolysed by intracellular esterases in live cells is converted to the strongly green fluorescent calcein (Ex 490 nm, Em 539 mm). After two days of cell culture no cytotoxic effect was observed and fibroblasts spread and colonized all the available area provided by the sample surface. In **Fig. 11**, a higher cell density in all plasma treated substrates was observed, in particular sample C, when compared with the untreated one. The results indicated that the coated samples composed by Hap and titanium oxide prepared by PEO method at a low applied voltage were cytocompatible and good substrates for cell growth. Therefore, they could be taken into consideration in the

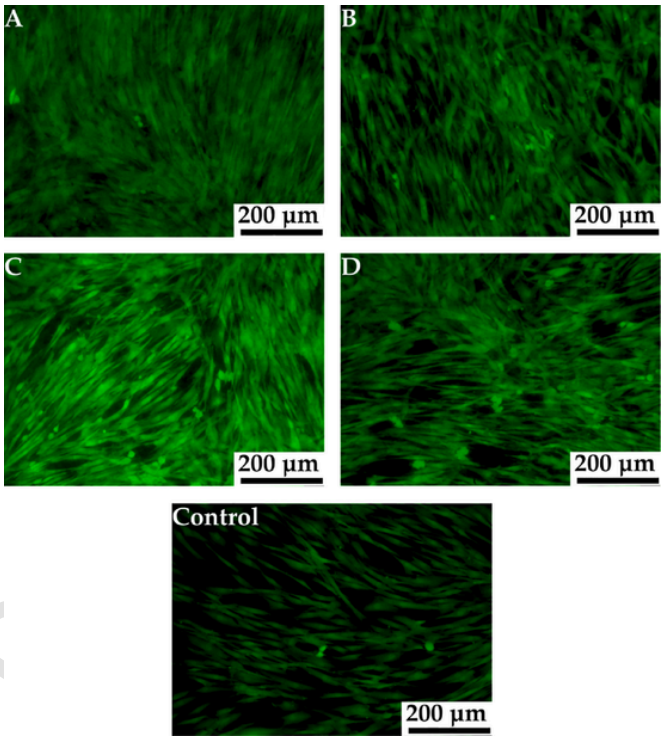


**Fig. 11.** Fluorescence microscope images on different representative samples showing the results of Calcein AM staining of skin fibroblasts after 48 h of direct culture on the surface of coated samples A, B, C and D and of positive control. The letters in the upper left corner indicate the corresponding samples.

generation of titanium implants suitable for bio medical applications, such as bone tissue engineering.

## 4. Conclusion

In this work, bioactive coatings on titanium alloy were successfully produced by PEO method working at low voltage (315 V), with consequent lower energy consumption in comparison with standard PEO treatments on Ti alloys. The coatings were mainly composed by Hap and titanium dioxide in two different crystalline forms (rutile and anatase). The addition of KOH induced the formation of a higher amount of rutile due to higher local temperatures. SEM micrographs showed that the bioactive coatings consisted of two or three different layers, an inner layer, which is characteristic of PEO coatings, and one or two porous layers (titanium oxide and Hap, with the last present as separate layer or as sealing of the pores of the PEO layer). The addition of KOH reduced the formation of the external Hap layer. The presence of PEO coatings remarkably improved cell adhesion and possibly proliferation, compared to the control untreated sample. Indeed, cell density appeared to be higher in tested samples than in the control surface. Also, all coated samples showed better corrosion properties than pure titanium, but it was noted that when pulsed mode was employed in the PEO process, a more porous inner layer was produced causing a reduction in the corrosion properties. Considering both corrosion properties and cell adhesion tests sample C appear to be the more promising for possible application as biomedical implant. The sample C was produced using direct current mode and the with the addition of KOH to the electrolyte.

## Declaration of Competing Interest

The authors declare that they have no known competing financial interests or personal relationships that could have appeared to influence the work reported in this paper.

## Acknowledgements

The authors want to thank the DeBio imaging Facility of the Department of Biology of the University of Padova for the cell adhesion tests.

## References

[1] A. Jaafar, C. Hecker, P. Árki, Y. Joseph, Sol-gel derived hydroxyapatite coatings for titanium implants: a review, Bioengineering 7 (2020) 1–23, https://doi.org/10.3390/bioengineering7040127.
[2] R.C. Rocha, A.G. de Sousa Galdino, S.N. da Silva, M.L.P. Machado, Surface, microstructural, and adhesion strength investigations of a bioactive hydroxyapatite-titanium oxide ceramic coating applied to Ti-6Al-4 V alloys by plasma thermal spraying, Mater. Res. 21 (2018), https://doi.org/10.1590/1980-5373-MR-2017-1144.
[3] N.T.T. Linh, P.D. Tuan, Characteristics of hydroxyapatite coating on Ti-6Al-4 V substrate fabricated via sequent H2O2-oxidizing and RF-sputtering processes, Vietnam J. Chem. 58 (2020) 654–660, https://doi.org/10.1002/vjch.202000064.
[4] C.A. Antônio, E.C. Rangel, S.F. Durrant, A. De Oliveira Delgado-Silva, M.H. Tabacniks, N.C. Da Cruz, Mg-containing hydroxyapatite coatings produced by plasma electrolytic oxidation of titanium, Mater. Res. 20 (2017) 891–898, https://doi.org/10.1590/1980-5373-MR-2016-0686.
[5] L.C. Zhang, L.Y. Chen, L. Wang, Surface Modification of Titanium and Titanium Alloys: technologies, Developments, and Future Interests, Adv. Eng. Mater. (2020) 22, https://doi.org/10.1002/adem.201901258.
[6] G. Mortazavi, J. Jiang, E.I. Meletis, Investigation of the plasma electrolytic oxidation mechanism of titanium, 2019. http://www.elsevier.com/open-access/userlicense/1.0/.
[7] M.A. Surmeneva, A. Vladescu, R.A. Surmenev, C.M. Pantilimon, M. Braic, C.M. Cotrut, Study on a hydrophobic Ti-doped hydroxyapatite coating for corrosion protection of a titanium based alloy, RSC Adv 6 (2016) 87665–87674, https://doi.org/10.1039/c6ra03397k.
[8] A.L. Yerokhin, X. Nie, A. Leyland, A. Matthews, Characterisation of oxide films produced by plasma electrolytic oxidation of a Ti6Al4V alloy, 2000.
[9] K. Kuroda, M. Okido, Hydroxyapatite coating of titanium implants using hydroprocessing and evaluation of their osteoconductivity, Bioinorg. Chem. Appl. (2012) 2012, https://doi.org/10.1155/2012/730693.
[10] S. Lugovskoy, B. Kazanski, N. Astashina, E.A. Vagner, Investigation of hydroxyapatite on Ti-6Al-4 V alloy prepared by plasma electrolytic oxidation, 2012. https://www.researchgate.net/publication/272239641.
[11] D.V. Mashtalyar, K.V. Nadaraia, A.S. Gnedenkov, I.M. Imshinetskiy, M.A. Piatkova, A.I. Pleshkova, E.A. Belov, V.S. Filonina, S.N. Suchkov, S.L. Sinebryukhov, S.V. Gnedenkov, Bioactive coatings formed on titanium by plasma electrolytic oxidation: composition and properties, Materials (Basel) 13 (2020), https://doi.org/10.3390/ma13184121 (Basel).
[12] S.A. Ulasevich, A.I. Kulak, S.K. Poznyak, S.A. Karpushenkov, A.D. Lisenkov, E.V. Skorb, Deposition of hydroxyapatite-incorporated TiO2 coating on titanium using plasma electrolytic oxidation coupled with electrophoretic deposition, RSC Adv 6 (2016) 62540–62544, https://doi.org/10.1039/c6ra10560b.
[13] S. Bharati, M.K. Sinha, D. Basu, Hydroxyapatite coating by biomimetic method on titanium alloy using concentrated SBF, 2005.
[14] C.J. Chung, R.T. Su, H.J. Chu, H. Te Chen, H.K. Tsou, J.L. He, Plasma electrolytic oxidation of titanium and improvement in osseointegration, J. Biomed. Mater. Res. - Part B Appl. Biomater. 101 B (2013) 1023–1030, https://doi.org/10.1002/jbm.b.32912.
[15] S. Durdu, Ö.F. Deniz, I. Kutbay, M. Usta, Characterization and formation of hydroxyapatite on Ti6Al4V coated by plasma electrolytic oxidation, J. Alloys Compd. 551 (2013) 422–429, https://doi.org/10.1016/j.jallcom.2012.11.024.
[16] D. Dzhurinskiy, Y. Gao, W.K. Yeung, E. Strumban, V. Leshchinsky, P.J. Chu, A. Matthews, A. Yerokhin, R.G. Maev, Characterization and corrosion evaluation of TiO2:n-HA coatings on titanium alloy formed by plasma electrolytic oxidation, Surf. Coatings Technol. 269 (2015) 258–265, https://doi.org/10.1016/j.surfcoat.2015.01.022.
[17] P. Hartjen, A. Hoffmann, A. Henningsen, M. Barbeck, A. Kopp, L. Kluwe, C. Precht, O. Quatela, R. Gaudin, M. Heiland, R.E. Friedrich, C. Knipfer, D. Grubeanu, R. Smeets, O. Jung, Plasma electrolytic oxidation of titanium implant surfaces: microgroove-structures improve cellular adhesion and viability, In Vivo (Brooklyn) 32 (2018) 241–247, https://doi.org/10.21873/invivo.11230.
[18] H.W. Kim, Y.H. Koh, L.H. Li, S. Lee, H.E. Kim, Hydroxyapatite coating on titanium substrate with titania buffer layer processed by sol-gel method, Biomaterials 25 (2004) 2533–2538, https://doi.org/10.1016/j.biomaterials.2003.09.041.
[19] C. Garcia-Cabezón, M.L. Rodriguez-Mendez, V.A. Borrás, B. Raquel, J.C.R. Cabello, A.I. Fonseca, F. Martin-Pedrosa, Application of plasma electrolytic oxidation coating on powder metallurgy Ti-6Al-4 V for dental implants, Metals (Basel). 10 (2020) 1–15, https://doi.org/10.3390/met10091167.
[20] R.V. Pohrelyuk, O.V. Proskurnyak, Y.V. Tкachuk, Obukh, Formation of Hydroxyapatite Coatings on Titanium by Plasma-Electrolytic Oxidation in Alkaline Electrolytes, Mater. Sci 55 (2020) 563–568, https://doi.org/10.1007/s11003-020-00339-8.
[21] F. Hanna, Z.A. Hamid, Electrodeposition of biomedical hydroxyapatite coatings on titanium alloy substrate, Pigment Resin Technol 32 (2003) 319–325, https://doi.org/10.1108/03699420310497463.
[22] T.H. Teh, A. Berkani, S. Mato, P. Skeldon, G.E. Thompson, H. Habazaki, K. Shimizu, Initial stages of plasma electrolytic oxidation of titanium, Corros. Sci. 45 (2003) 2757–2768, https://doi.org/10.1016/S0010-938X(03)00101-X.
[23] A. Krząkała, A. Kazek-Kęsik, W. Simka, Application of plasma electrolytic oxidation to bioactive surface formation on titanium and its alloys, RSC Adv 3 (2013) 19725–19743, https://doi.org/10.1039/c3ra43465f.
[24] S. Aliasghari, P. Skeleton, G.E. Thompson, Plasma electrolytic oxidation of titanium in a phosphate/silicate electrolyte and tribological performance of the coatings, Appl. Surf. Sci. 316 (2014) 463–476, https://doi.org/10.1016/j.apsusc.2014.08.037.
[25] L. Pezzato, P. Cerchier, K. Brunelli, A. Bartolozzi, R. Bertani, M. Dabalà, Plasma electrolytic oxidation coatings with fungicidal properties*, Surf. Eng. 35 (2019) 325–333, https://doi.org/10.1080/02670844.2018.1441659.
[26] L. Pezzato, K. Brunelli, S. Diodati, M. Pigato, M. Bonesso, M. Dabalà, Microstructural and corrosion properties of hydroxyapatite containing peo coating produced on az31 mg alloy, Materials (Basel) 14 (2021), https://doi.org/10.3390/ma14061531.
[27] A. Santos-Coquillat, E. Martínez-Campos, H. Mor. Sánchez, L. Moreno, R. Arrabal, M. Mohedano, A. Gallardo, J. Rodríguez-Hernández, E. Matykina, Hybrid functionalized coatings on Metallic Biomaterials for Tissue Engineering, Surf. Coatings Technol 422 (2021), https://doi.org/10.1016/j.surfcoat.2021.127508.
[28] A. Fattah-alhosseini, M. Molaei, K. Babaei, The effects of nano- and micro-particles on properties of plasma electrolytic oxidation (PEO) coatings applied on titanium substrates, A review, Surfaces and Interfaces 21 (2020) 100659, https://doi.org/10.1016/j.surfin.2020.100659.
[29] P. Cerchier, L. Pezzato, K. Brunelli, P. Dolcet, A. Bartolozzi, R. Bertani, M. Dabalà, Antibacterial effect of PEO coating with silver on AA7075, Mater. Sci. Eng. C. 75 (2017) 554–564, https://doi.org/10.1016/j.msec.2017.02.084.
[30] A. Sobolev, M. Zinigrad, K. Borodianskiy, Ceramic coating on Ti-6Al-4 V by plasma electrolytic oxidation in molten salt: development and characterization, Surf. Coatings Technol. 408 (2021) 126847, https://doi.org/10.1016/j.surfcoat.2021.126847.
[31] A. Sobolev, I. Wolicki, A. Kossenko, M. Zinigrad, K. Borodianskiy, Coating formation on Ti-6Al-4 V alloy by Micro Arc Oxidation in molten salt, Materials (Basel) 11 (2018) 4–11, https://doi.org/10.3390/ma11091611.
[32] J. Sun, Y. Han, X. Huang, Hydroxyapatite coatings prepared by micro-arc oxidation in Ca- and P-containing electrolyte, Surf. Coatings Technol. 201 (2007) 5655–5658, https://doi.org/10.1016/j.surfcoat.2006.07.052.
[33] L. Pezzato, M. Dabalà, S. Gross, K. Brunelli, Effect of microstructure and porosity of AlSi10Mg alloy produced by selective laser melting on the corrosion properties of plasma electrolytic oxidation coatings, Surf. Coatings Technol. 404 (2020) 126477, https://doi.org/10.1016/j.surfcoat.2020.126477.
[34] A. Fattah-alhosseini, M. Molaei, N. Attarzadeh, K. Babaei, F. Attarzadeh, On the enhanced antibacterial activity of plasma electrolytic oxidation (PEO) coatings that incorporate particles: a review, Ceram. Int. 46 (2020) 20587–20607, https://doi.org/10.1016/j.ceramint.2020.05.206.
[35] M. Molaei, M. Nouri, K. Babaei, A. Fattah-Alhosseini, Improving surface features of PEO coatings on titanium and titanium alloys with zirconia particles: a review, Surfaces and Interfaces 22 (2021) 100888, https://doi.org/10.1016/j.surfin.2020.100888.
[36] M. Molaei, A. Fattah-alhosseini, M. Nouri, A. Nourian, Systematic optimization of corrosion, bioactivity, and biocompatibility behaviors of calcium-phosphate plasma electrolytic oxidation (PEO) coatings on titanium substrates, Ceram. Int. (2021), https://doi.org/10.1016/j.ceramint.2021.11.175.
[37] P. Pesode, S. Barve, Surface modification of titanium and titanium alloy by plasma electrolytic oxidation process for biomedical applications: a review, Mater. Today Proc. 46 (2021) 594–602, https://doi.org/10.1016/j.matpr.2020.11.294.
[38] N. Huang, Y.X. Leng, P.D. Ding, Surface engineered titanium alloys for biomedical devices, 2010. https://doi.org/10.1533/9781845699451.3.568.
[39] E. MATYKINA, R. ARRABAL, M. MOHEDANO, B. MINGO, J. GONZALEZ, A. PARDO, M.C. MERINO, Recent advances in energy efficient PEO processing of aluminium alloys, Trans. Nonferrous Met. Soc. China (English Ed. 27 (2017) 1439–1454, https://doi.org/10.1016/S1003-6326(17)60166-3.
[40] M. Mohedano, B. Mingo, H. Mora-Sánchez, E. Matykina, R. Arrabal, Effects of pre-anodizing and phosphates on energy consumption and corrosion performance of PEO coatings on AA6082, Surf. Coatings Technol. 409 (2021), https://doi.org/10.1016/j.surfcoat.2021.126892.
[41] M. Aliofkhazraei, D.D. Macdonald, E. Matykina, E.V. Parfenov, V.S. Egorkin, J.A. Curran, S.C. Troughton, S.L. Sinebryukhov, S.V. Gnedenkov, T. Lampke, F. Simchen, H.F. Nabavi, Review of plasma electrolytic oxidation of titanium substrates: mechanism, properties, applications and limitations, Appl. Surf. Sci. Adv. 5 (2021) 100121, https://doi.org/10.1016/j.apsadv.2021.100121.
[42] N. Attarzadeh, C.V. Ramana, Plasma electrolytic oxidation ceramic coatings on zirconium (Zr) and zr-alloys: part-ii: properties and applications, Coatings (2021) 11, https://doi.org/10.3390/coatings11060620.
[43] M.S. Kim, J.J. Ryu, Y.M. Sung, One-step approach for nano-crystalline hydroxyapatite coating on titanium via micro-arc oxidation, Electrochem. Commun. 9 (2007) 1886–1891, https://doi.org/10.1016/j.elecom.2007.04.023.
[44] L. Pezzato, L.B. Coelho, R. Bertolini, A.G. Settimi, K. Brunelli, M. Olivier, M. Dabalà, Corrosion and mechanical properties of plasma electrolytic oxidation-coated AZ80 magnesium alloy, Mater. Corros. 70 (2019) 2103–2112, https://doi.org/10.1002/maco.201910847.
[45] M. Laveissière, H. Cerda, J. Roche, L. Cassayre, L. Arurault, In-depth study of the influence of electrolyte composition on coatings prepared by plasma electrolytic oxidation of TA6V alloy, Surf. Coatings Technol. 361 (2019) 50–62, https://doi.org/10.1016/j.surfcoat.2018.12.122.